

RESEARCH ARTICLE

Glucosamine-phosphate N-acetyltransferase 1 and its DNA methylation can be biomarkers for the diagnosis and prognosis of lung cancer

Peikun Ding | Bin Peng | Guofeng Li  | Xuefeng Sun | Guangsuo Wang

Department of Thoracic Surgery,
Shenzhen People's Hospital, The
Second Clinical Medical College of Jinan
University

Correspondence

Guofeng Li, Xuefeng Sun and Guangsuo
Wang, Department of Thoracic Surgery,
Shenzhen People's Hospital, The
Second Clinical Medical College of Jinan
University, No. 1017, Dongmen North
Road, Luohu District, Shenzhen, 518020,
China.

Emails: lgf127@tom.com; sunxuefeng_sxf@163.com; wangguangsuo_wgs@163.com

Funding information

Shenzhen Key Medical Discipline
Construction Fund, Grant/Award Number:
No.SZXK018

Abstract

Objective: Lung cancer ranking high in the cancer-related list has long perplexed patients, in which glucosamine-phosphate N-acetyltransferase 1 (GNPNAT1) is found to be highly expressed. Besides, DNA methylation is perceived as a biomarker to assess the prognosis of patients with various cancers. However, the correlation between GNPAT1 and DNA methylation and the role of GNPAT1 in lung cancer remain vague.

Methods: Principal component analysis (PCA), heatmap, volcano map, Venn diagram, gene ontology (GO), and Kyoto Encyclopedia of Genes and Genomes (KEGG) analysis were used to screen out the candidate genes. The viability, migration, and invasion of lung cancer cells were detected by CCK-8 and Transwell assays. An xenograft tumor mouse model was established. The relative expressions of GNPAT1, E-cadherin, vimentin, Matrix metalloproteinase-2 (MMP-2), tissue inhibitor of metalloproteinase-2 (TIMP-2), E2F1, and cyclin D1 in cells or xenograft tumor tissues were quantified by Western blot, RT-qPCR, or immunohistochemistry assay.

Results: GNPAT1 was screened as the research object. GNPAT1 methylation was downregulated, while GNPAT1 expression was upregulated in lung cancer tissues. The methylation and mRNA levels of GNPAT1 were correlated with the patient prognosis. GNPAT1 increased cell viability, migration and invasion, and promoted the xenograft tumor volume and weight, whereas shGNPNAT1 acted oppositely. Moreover, expressions of Vimentin, MMP-2, E2F1, and cyclin D1 were increased, but E-cadherin and TIMP-2 expressions were decreased by overexpressed GNPAT1, whilst GNPAT1 knockdown ran conversely.

Conclusion: GNPAT1 and methylated GNPAT1 coverage are biomarkers for the diagnosis and prognosis of lung cancer.

KEYWORDS

Biomarker, DNA methylation, GNPAT1, Lung cancer, Prognosis

Peikun Ding and Bin Peng Co-first authors and contributed equally.

This is an open access article under the terms of the [Creative Commons Attribution-NonCommercial-NoDerivs](https://creativecommons.org/licenses/by-nc-nd/4.0/) License, which permits use and distribution in any medium, provided the original work is properly cited, the use is non-commercial and no modifications or adaptations are made.

© 2022 The Authors. *Journal of Clinical Laboratory Analysis* published by Wiley Periodicals LLC.

1 | INTRODUCTION

Lung cancer persistently ranks high in the cancer-related list, with high morbidity and mortality worldwide, based on the released data by WHO.¹ The survival rate of patients suffering from lung cancer is primarily dependent on the stage of diagnosis.² As reflected in the most recent data on population-oriented lung cancer survival rate, the Figure 6% mirrors the embarrassing status of largely proportioned patients perplexed by metastatic disease. Nonetheless, early diagnosis of this disease could be contributing to prognosis improvement.³

Pushed by technological revolution, biomedicine is impelled by genomics, metabolomics, proteomics, and bioinformatics. Thereinto, a growing number of researchers show overriding interest in the study of biomarkers that can be evaluated as an index of biological, pathogenic, or pharmacologic response toward an intervention⁴ and the dedicated roles in the detection, diagnosis, treatment, and prognosis of lung cancer.⁵ During the process of chasing latent biomarkers for lung cancer, the global DNA hypomethylation with cytosine-phosphoric acid-guanine (CPG) island sequences hypermethylated in the promoter regions of tumor suppressor genes are becoming more prominent, which are the features of tumor tissue.⁶

DNA methylation involves the transfer of a methyl group to the fifth carbon of the cytosine to form 5-methylcytosine (5mC) under the catalysis of DNA methyltransferases (Dnmts).⁷ Appropriate DNA methylation functions in cell differentiation, embryonic development, and genome stability,⁸ while aberrant DNA methylation indicates an epigenetic change and even signifies tumor suppressor gene inactivation if the change takes place in gene promoter region.⁹ The level of methylation is regarded as a workable biomarker to assess prognosis, disease recurrence, early detection or risk estimation, or indeed as a therapeutic target.¹⁰ DNA methylation has exhibited its potential as a marker for cancer diagnosis and prognosis, including lung cancer.¹¹

Based on bioinformatic analysis, we selected glucosamine-phosphate N-acetyltransferase 1 (GNPNAT1) as our candidate for DNA methylation study. As a pivotal enzyme in hexosamine biosynthetic pathway (HBP) that is one of the important glycometabolism pathways in glycolysis,¹² GNPAT1 has been proved to be one of the metabolic indicators in predicting the prognosis of tumor patients.^{13,14} For tumor cells, metabolism is disordered due to the dysfunction of tumor suppressor genes or the activation of oncogenes,¹³ with the incremental glucose as a partial manifestation.^{15,16} A prior research uncovered that GNPAT1 plays an independent prognostic role in lung adenocarcinoma (LUAD) by comparing its expression in tumor and adjacent tissues,² echoed with another research reporting that GNPAT1 is highly expressed in LUAD and may be a potential prognostic biomarker for LUAD.¹² However, whether GNPAT1 is a biomarker for lung cancer and the biological function it performs remain vague. Besides, studies and clinical data regarding the association of GNPAT1 with DNA methylation are limited, although GNPAT1 is a promising candidate.

Herein, we conducted a deeper research toward DNA methylation and delved into the effects of GNPAT1 and its methylation in the progression of lung cancer, aiming to seek a potentially prognostic and therapeutic biomarker for lung cancer.

2 | MATERIALS AND METHODS

2.1 | Ethics statement

Animal experiments were approved by the Medical Ethics Committee of Shenzhen People's Hospital (approval number: LL-KY-2022022). The clinical data were obtained from 60 lung cancer patients who were treated in Shenzhen People's Hospital. All the patients signed the written informed consents and agreed that their lung cancer tissues would be applied in our research.

2.2 | Bioinformatic analysis

RNA-seq, methylation-related data, and clinical information were downloaded from the Cancer Genome Atlas (TCGA) database. The Chip Analysis Methylation Pipeline (ChAMP) package including quality control metrics and a selection of normalization methods was adopted to identify differentially methylated regions. Then, principal component analysis (PCA) and heatmap were used to remove the outliers, and 26 pairs of matched methylated samples were then obtained. Subsequently, PCA and heatmap (unsupervised clustering heatmap) were re-made based on the top 1000 probe sites with the largest variance. Further, differential expression analysis towards expression matrix of the samples was carried out via ChAMP package, differential methylated points (DMPs) with $\Delta\beta > 0.2$ and False Discovery Rate (FDR) < 0.05 were screened as threshold, and volcano plot as well as heat map (unsupervised clustering heatmap) were then made. Next, differential expression analysis towards RNA-seq via edgeR was conducted and differentially expressed genes (DEGs) were obtained under the standard of FDR < 0.05 and $\log_2FC > 1$. Besides, the intersected genes between DMPs corresponding genes and DEGs which were exhibited by VennDiagram package were acquired, genes existing in both hyper_DMPs and hypo_DMPs regions where settled both hyper-methylated and hypo-methylated genes were removed, and 268 hyper-methylated genes in down-genes region and 213 hypo-methylated genes in up-genes region were ultimately gained. Next, 417 methylation-driving genes were harvested, whose expression trends were inconsistent with their methylation trends and negatively correlated with spearman coefficient, with p value < 0.05 . Afterward, the targets were input into the Database for Annotation, Visualization and Integrated Discovery (DAVID) v6.8¹⁷ for GO analysis comprising biological process (BP), molecular function (MF), and cell component (CC), and Kyoto Encyclopedia of Genes and Genomes (KEGG) analysis was subsequently implemented toward the harvests to select the candidate genes.

2.3 | Determination of GNPAT1 DNA methylation level

The DNA methylation level of GNPAT1 in Formalin-Fixed and Paraffin Embedded (FFPE) specimens was detected through NMPA (China National Medical Products Administration)-marked in vitro diagnostic (IVD) test LungMe® assay (20,173,403,354, Tellgen Co.).

Tissue genomic DNA (gDNA) was isolated from FFPE samples via the FFPE DNA extraction kit (56,404, Qiagen, Hilden). Next, the concentration of extracted DNA was measured through the highly sensitive Qubit assay (Qubit Fluorometer, Q33327, Thermo Fisher Scientific; High sensitive fluorescent dye, Q32850, Thermofisher). Fifty ng DNA/sample was treated with sodium bisulfite using the Tellgen DNA purification kit (PF03X056, Tellgen Co.). After purification, the bisulfite-converted DNA was amplified by methylation specific real-time PCR (MS-PCR) amplification using LungMe® real-time PCR kit as described before.¹⁸ The MS-PCR was used to amplify methylated GNPAT1, and PCR amplification was performed in an ABI 7500 real-time PCR instrument (4,351,107, Applied Biosystems), and SDS Software (SDS v1.4.1, Applied Biosystems) was selected to analyze the results. The relative level of methylated GNPAT1 was calculated according to the delta cycle threshold ΔCt .¹⁹

2.4 | Cell culture and treatment

Two cell lines, A549 (CCL-185) and H1299 (CRL-5803) used in this study, were purchased from American type culture collection (ATCC). Cells were cultured in Dulbecco's modified Eagle's medium (DMEM) (31331093, Gibco) supplemented with 10% fetal bovine serum (FBS) (12664025, Gibco), 2 mM L-glutamine (G7513, Sigma-Aldrich), 100 U/ml penicillin, and 100 $\mu\text{g}/\text{ml}$ streptomycin (15070063, Thermo Fisher Scientific) in an incubator (51030286, Thermo Fisher Scientific) under a humidified atmosphere of 5% CO_2 at 37°C.

2.5 | Cell transfection and grouping

Cells were transfected with short hairpin RNAs targeting GNPAT1 (including shRNA1 and shRNA2) and GNPAT1 overexpression plasmid. With this method, four groups were established as follows: control, shRNA1, shRNA2, and GNPAT1 groups. In our study, GNPAT1 overexpression plasmid and GNPAT1 shRNA were all synthesized by GenePharma (Shanghai, China). In brief, cells were cultured in 6-well plates till 90% confluence was reached, and then the culture medium was removed. After being washed with PBS, cells were transfected with the above plasmids using Lipofectamine 2000 (11,668,027, Thermo Fisher Scientific) based on the manufacturer's directions. Transfection efficiency

was assessed after 24 h (h) of incubation under a humidified atmosphere of 5% CO_2 at 37°C.

2.6 | Cell counting kit-8 (CCK-8) assay

Cell viability was measured via CCK-8 kit (C0037, Beyotime) in accordance with manufacturer's protocols. Simply put, transfected cells were seeded into 96-well plates at a density of $2 \times 10^3/\text{well}$ and cultured for 24, 48, and 72 h. Then, 10 μl of CCK-8 solution was added into every well and incubated for 2 h, and the optical density (OD) was measured at a wavelength of 450 nm via a microplate reader (Varioskan LUX).

2.7 | Real-time quantitative polymerase chain reaction (RT-qPCR)

Relative GNPAT1 mRNA expression was measured by RT-qPCR. Briefly, total RNAs were extracted via Trizol reagent (T9424, Sigma-Aldrich), whose quantities and purities were determined by a spectrophotometer (ND-LITE-PR, Thermo Fisher Scientific) and reversely transcribed by a transcriptase kit (K1621, Thermo Fisher Scientific) in accordance with the manufacturer's instructions. Next, RT-qPCR experiment was carried out with the help of SYBR PremixEx Taq II Kit (RR820L, TaKaRa) in LightCycler 480-II System (RocheDiagnostics). The RT-qPCR amplification conditions were listed as follows: 95°C for 5 min; 40 cycles of 95°C for 5 seconds(sec), 60°C for 20s, and 72°C for 40s. The forward (F) and reverse (R) primer sequences are described below: for GNPAT1, CCCCAACACATCCTGGAGAA (F) and TGCCAAGCTGCTTCTCTG (R); for GAPDH, CACCATCTCCAGGAGCGAG (F) and CTCAGTGTAGCC CAGGATGC (R). The comparative delta Ct (ΔCt) method was adopted to analyze GNPAT1 differential mRNA expression in normal and cancer cells. $2^{-\Delta\Delta\text{Ct}}$ method was adopted¹⁹ to calculate the results, with GAPDH serving as the internal reference.

2.8 | Cell migration and invasion assays

Migration and invasion assays were conducted in 24-well Transwell chamber (8 μm pore size; 140,629, Thermo Fisher Scientific) pre-coated without or with Matrigel (356,234, BD Bioscience). After 48 h of transfection, 5×10^4 A549 or H1299 cells were placed into the upper chamber containing serum-free DMEM (200 μl) for migration or invasion assay. DMEM (600 μl) supplemented with 10% FBS was placed into the lower chamber. After 48 h of incubation, cells remaining in the upper chamber were wiped off, while cells that migrated or invaded through the pores to the lower chamber were fixed with 4% paraformaldehyde (158,127, Sigma-Aldrich), and then stained with 0.1% crystal violet (V5265, Sigma-Aldrich). Finally, the number of

stained cells was counted under a microscope (IXplore Pro, Olympus Corporation).

2.9 | Animal experiments

A total of 36 six-week-old male BALB/c nude mice were bought from ALF Biotechnology and housed in a specific pathogen-free condition for 5 days. The mice were divided into six groups ($n = 6/\text{group}$): two control groups, two GNPAT1 groups, and two shRNA1 groups. Mice in the GNPAT1 or shRNA1 groups were subcutaneously injected with 1×10^6 A549 cells/H1299 cells with transfection of GNPAT1 plasmid and shRNA for GNPAT1 (shGNPNAT1). Then, all mice were normally housed for 28 days. On the last day, after the mice were sacrificed with isoflurane (R510-22, RWD, Shenzhen, China), their tumor tissues were collected, subsequent to which the tumor weight and tumor volume (volume = $\pi \times \text{tumor length} \times \text{tumor width}^2/6$) were recorded.

2.10 | Western blot assay

Protein expressions of GNPAT1, E-cadherin, vimentin, Matrix metalloproteinase-2 (MMP-2), tissue inhibitor of metalloproteinase-2 (TIMP-2), E2F1, and cyclin D1 were measured by Western blot. The total proteins from cells and tumor tissues were first isolated using RIPA lysis buffer (20-188, Sigma-Aldrich). Then, the protein concentration was quantified by the BCA assay kit (P0011, Beyotime) based on manufacturer's instructions after lysate was centrifuged. Subsequently, the proteins at gross weight of $30 \mu\text{g}$ were resolved in 10% SDS-PAGE and then transferred onto PVDF membranes (FFP28, Beyotime). After being blocked with 5% skimmed milk at room temperature for 1 h, the membranes were incubated with the primary antibodies against GNPAT1 (rabbit, 1:2000, 21 kDa, ab234981, Abcam, Cambridge, UK), E-Cadherin (rabbit, 1:20000, 97 kDa, ab40772, Abcam), Vimentin (rabbit, 1:2000, 54 kDa, ab92547, Abcam), MMP2 (rabbit, 1 $\mu\text{g}/\text{mL}$, 72 kDa, ab37150, Abcam), TIMP-2 (rabbit, 1:1000, 24 kDa, ab180630, Abcam), E2F1 (rabbit, 1:2000, 47 kDa, ab179445,

Abcam), cyclin D1 (rabbit, 1:20000, 34 kDa, ab134175, Abcam), and GAPDH (rabbit, 1:10000, 36 kDa, ab181602, Abcam). Afterward, the membranes were thereupon incubated with horse-radish peroxidase (HRP)-conjugated secondary antibody goat anti-rabbit IgG (1:3000, ab6721, Abcam). Protein signals were tested and collected via enhanced chemiluminescence (ECL) Kit (P0018S, Beyotime) and were quantified through the Image J software (Image J 1.8.0).

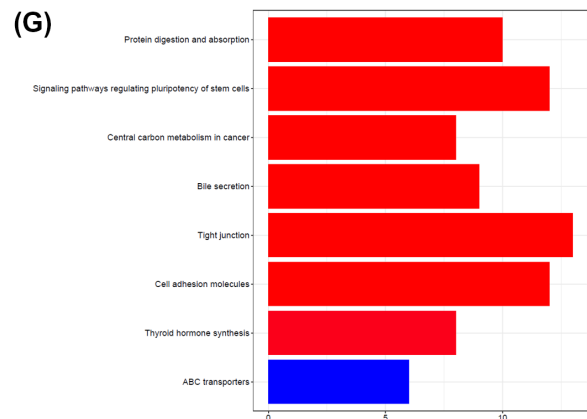
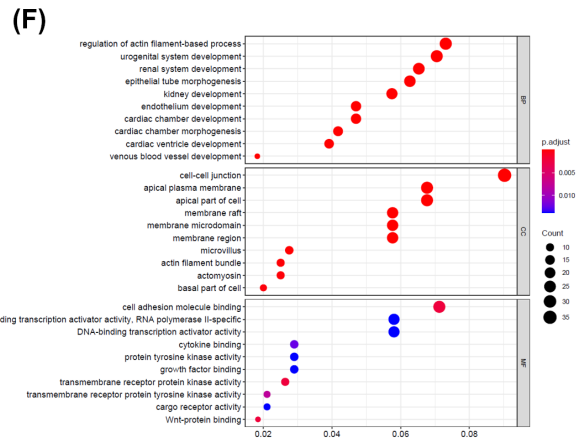
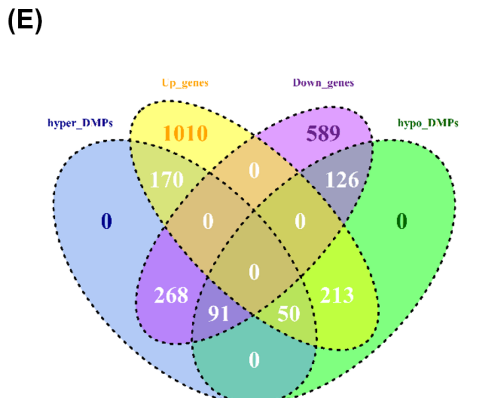
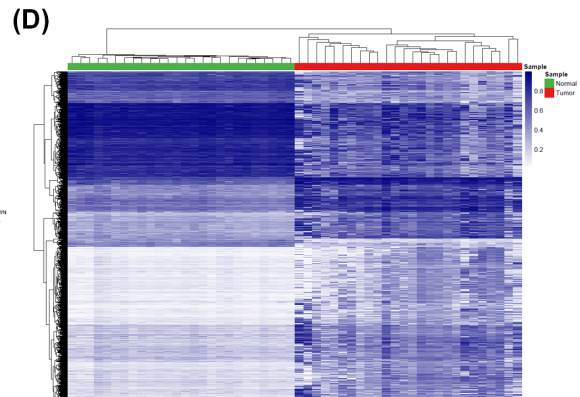
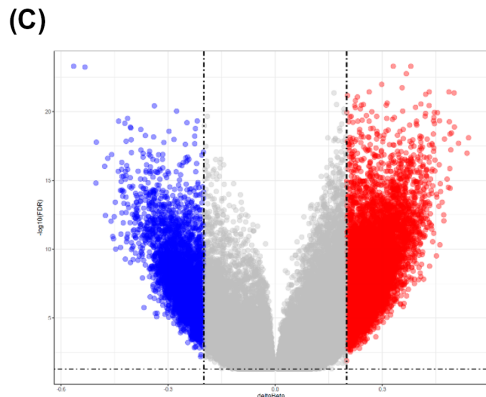
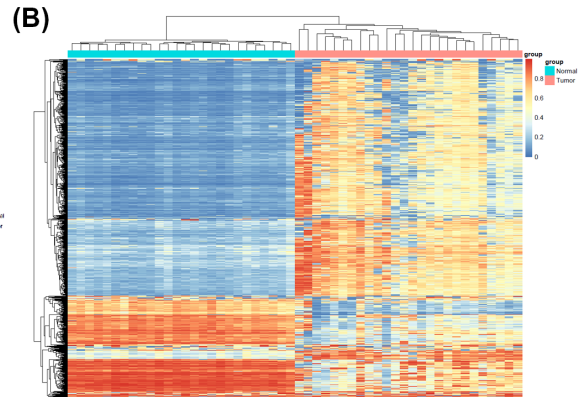
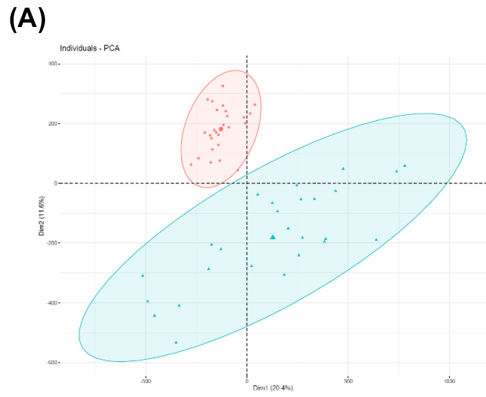
2.11 | Immunohistochemistry assay

The expression of GNPAT1 in mice tumor tissues was analyzed through immunohistochemistry assay. Briefly, the collected tumor tissue was fixed with 4% tissue fixative (P1110, Solarbio), dehydrated with gradient alcohol, and then transparently treated with xylene (50,009, Meryer). Subsequently, the tissue was embedded into paraffin (M27079, Meryer) and sectioned into $4 \mu\text{m}$ slices. After being dewaxed, the tissue slices were added with antigen retrieval buffer (C1032, Solarbio) and goat serum (16,210,064, Thermo Fisher Scientific). Subsequently, the tissue slices were incubated with anti-GNPAT1 antibody (ab234981, Abcam) at 4°C overnight, followed by further incubation with goat anti-rabbit IgG (ab205718, Abcam) for 1 h. Then, the tissue slices were colored by DBA buffer (SFQ004, 4A Biotech, Beijing, China) and haematoxylin (H8070, Solarbio) and further treated with gradient alcohol, xylene, and neutral gum (G8590, Solarbio). Lastly, the GNPAT1-positive cells in the tissue slices were observed using a THUNDER tissue microscope at a magnification of $100\times$.

2.12 | Statistics analysis

Statistical analyses were conducted by IBM SPSS 22.0 software (SPSS). Data were enumerated via Chi square test or rank sum test and expressed as mean \pm standard deviation (SD). Paired t test and one-way analysis of variance (ANOVA) were used to analyze the data from two or more groups. For measurements, $p < 0.05$ was considered statistically significant.

FIGURE 1 GNPAT1 was selected as the candidate gene after screening. (A, B) PCA and heatmap were based on the top 1000 probe sites with the largest variance after removal of the outliers, and the final 26 pairs of matched methylated samples were obtained. In PCA, pink circles were for the normal group and blue triangles were for the tumor group. In heatmap, the red color indicated upregulated genes, while the blue color signified downregulated genes. (C, D) Volcano plot displayed the pattern of upregulated and downregulated genes, and a clustering heatmap indicated the varied expression of genes in two groups after the deep filtration of DMPs with $\Delta\beta > 0.2$ and $\text{FDR} < 0.05$ as threshold. The red dots in the left plot represented upregulated genes, blue dots denoted downregulated genes with statistical significance, and gray dots exhibited no differentially expressed genes of DMPs. The dark blue in the right plot indicated up-regulated genes, while the light blue color signified down-regulated genes. (E) The Venn Diagram analysis was conducted to determine the intersection of DMPs and DEGs under the screening standard of $\text{FDR} < 0.05$ and $\log_2\text{FC} > 1$. Methylation-driving genes were harvested after differential expression analysis towards RNA-seq via edgeR. (F, G) GO and KEGG pathway analyses were carried out for predicting the differentially expressed genes. The y-coordinate in (F) represented the GO entry, and the abscissa was the ratio of genes enriched on the GO entry to the total target genes. The color in the right side indicated the size of the p value, while the bubble size represents the number of genes enriched on the modified GO entry. PCA: principal component analysis, FDR: False Discovery Rate, DMPs: differential methylated points, DEGs, differentially expressed genes, GO, Gene ontology, Kyoto Encyclopedia of Genes and Genomes.



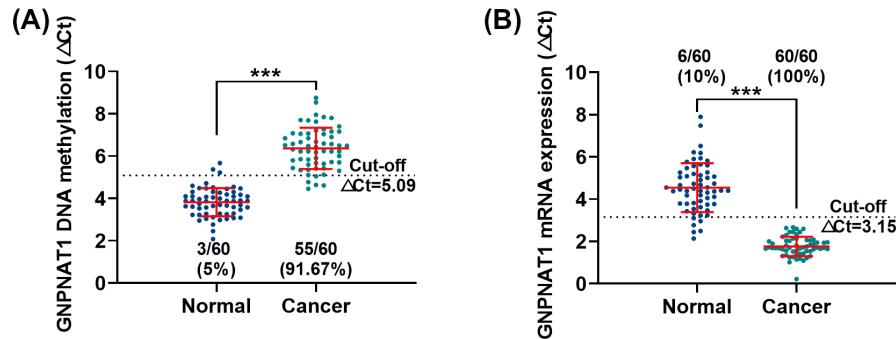


FIGURE 2 GNPAT1 methylation level was downregulated in carcinoma tissue. (A) Δ Ct value in the cancer group was greater than that in the normal group, indicating that GNPAT1 DNA methylation coverage in cancer group was less than that in the normal group. (B) Δ Ct value in the normal group was greater than that in the cancer group, demonstrating that GNPAT1 mRNA was less expressed in the normal group than that in the cancer group. *** $p < 0.001$ vs. Normal. All results represent as means \pm standard deviation (SD) of triplicate determinations. GNPAT1: glucosamine-phosphate N-acetyltransferase 1.

3 | RESULTS

3.1 | PCA, cluster, and volcano plot analysis

PCA was applied to determine the classification performance of the identified differentially methylated DNA regions. The results showed that the sum of variation (percent) by Dim1 was 20.4% and by Dim2 was 11.6%. Meanwhile, we observed that the normal and the tumor samples were effectively separated (Figure 1A). Then, a heatmap of clustering analysis was constructed. As depicted in Figure 1B, the right side of the samples was the tumor group, and the left half was the normal group. Thereinto, the red color indicated major abundance, and the blue color denoted minor abundance (Figure 1B). The heatmap of the top 1000 probe sites illustrated a massive difference of DNA methylation situation between the tumor and the normal samples (Figure 1B). A volcano plot displayed the pattern of DMPs, including upregulated and downregulated genes (Figure 1C). Additionally, the clustering heatmap indicated the expression of DMPs in the tumor group was significantly different from that of the normal group (Figure 1D) after the deep filtration.

3.2 | Venn Diagram, GO, and KEGG pathway enrichment analyses

For DMP datasheet, total number of 918 was identified, including 339 in hypo area, 141 overlapped and 438 in hyper area (Figure 1E). For DEG datasheet, 2517 DEGs were acquired, including 1443 up-regulated genes and 1074 downregulated genes (Figure 1E). Venn Diagram analysis was conducted to determine the intersection of DMPs and DEGs (Figure 1E). By removing genes existing in both hyper_DMPs and hypo_DMPs regions where settled both hyper-methylated and hypo-methylated genes, we obtained 268 hypermethylated genes in down-genes region and 213 hypo-methylated genes in up-genes region. Finally, we harvested 417

methylation-driving genes whose expression trends were inconsistent with their methylation trends and negatively correlated with spearman coefficient, with p value < 0.05 .

For BP, the top 5 influence factors are regulation of actin filament-based process, urogenital system development, renal system development, epithelial tube morphogenesis, and kidney development. In terms of CC, the top 5 influence factors are cell-cell junction, apical plasma membrane, apical part of cell, membrane raft, and microdomain. With regard to MF, the top 5 influence factors are cell adhesion molecule binding, DNA-binding transcription activator activity and RNA polymerase II-specific, DNA-binding transcription activator activity, cytokine binding, and protein tyrosine kinase activity (Figure 1F). Besides, DAVID v6.8¹⁷ was used for KEGG analysis against the targets. Subsequently, the top 8 signaling pathways with significant P values were selected, and top 5 influence factors included tight junction, signaling pathways regulating pluripotency of stem cells, cell adhesion molecules, protein digestion and absorption, and bile secretion (Figure 1G). GNPAT1 was selected as the candidate gene for further analysis (Figure 1A–G).

3.3 | GNPAT1 methylation and mRNA expression in carcinoma and para-carcinoma tissues

We classified the samples into either cancer group or the normal group to see the differences between carcinoma and para-carcinoma tissues via Δ Ct calculation and comparison based on the principle that the greater the Δ Ct value is, the smaller the methylated coverage is.²⁰ Δ Ct value in the cancer group was greater than that in the normal group, indicating that GNPAT1 DNA methylation coverage in cancer group was less than that in the normal group (Figure 2A, $p < 0.001$). Besides, we measured GNPAT1 mRNA expression in both groups and found the PCR Δ Ct value in the normal group was greater than that in the cancer group, demonstrating that GNPAT1 mRNA was highly expressed in the cancer group (Figure 2B, $p < 0.001$).

3.4 | Correlation of GNPAT1 methylation and mRNA expression in clinical data

Here, we not only measured the GNPAT1 methylation level and mRNA expression in the lung cancer tissues but also referred to the clinical data regarding the clinicopathological features of lung cancer patients. The results manifested that the lower the methylation level of GNPAT1 (with higher ΔCt value), the worse the prognosis appeared. Meanwhile, the methylation level of GNPAT1 was linked to tumor size, clinical stages, and lymph node metastasis (Table 1, $p < 0.05$). In addition, we observed that the more the GNPAT1 expressed in cancer (with lower PCR ΔCt value), the worse the prognosis would be, and that the mRNA expression level of GNPAT1 was also associated with tumor size, clinical stages, and lymph node metastasis (Table 2, $p < 0.05$).

3.5 | GNPAT1 stimulated the viability, migration, and invasion of lung cancer cells

To further dig out the role of GNPAT1 in lung cancer, we conducted cell transfection experiment. The results showed that in both A549 and H1299 cells, GNPAT1 mRNA was significantly overexpressed in GNPAT1 group, while being less expressed in shRNA1

TABLE 1 The relationship between GNPAT1 methylation level and clinical characteristics of lung cancer patients

Variable	n	GNPAT1 methylation (ΔCt)		p value
		Low	High	
Total	60	30	30	
Age (years)				
≤60	27	14	13	0.795
>60	33	16	17	
Grade				
T1	31	17	14	0.559
T2	17	8	9	
T3	12	5	7	
Tumor size (cm)				
≤5	38	23	15	0.032
>5	22	7	15	
Clinical stages				
I+II	40	26	14	0.001
III+IV	20	4	16	
Lymph node metastasis				
Absent	35	25	10	0.000
Present	25	5	20	
Differentiation				
Well-Moderately	37	20	17	0.426
Poorly	23	10	13	

TABLE 2 The relationship between GNPAT1 mRNA expression and clinical characteristics of lung cancer patients

Variable	n	GNPAT1 expression (ΔCt)		p value
		Low	High	
Total	60	30	30	
Age (years)				
≤60	27	11	16	0.194
>60	33	19	14	
Grade				
T1	31	16	15	0.846
T2	17	8	9	
T3	12	6	6	
Tumor size (cm)				
≤5	38	13	25	0.001
>5	22	17	5	
Clinical stages				
I+II	40	15	25	0.006
III+IV	20	15	5	
Lymph node metastasis				
Absent	35	11	24	0.001
Present	25	19	6	
Differentiation				
Well-Moderately	37	19	18	0.791
Poorly	23	11	12	

and shRNA2 groups when compared with that in the control group (Figure 3A,B, $p < 0.05$), signifying the triumph of the transfection. Additionally, we performed cell viability, migration, and invasion tests to see the effect of GNPAT1 aberrant expression on the lung cancer cells. The results of CCK-8 assay revealed that OD value in GNPAT1 group was higher than that in control group, and OD value in shRNA1 and shRNA2 groups was lower than that in control group, suggesting that GNPAT1 overexpression reinforced yet GNPAT1 knockdown impaired cell viability (Figure 3C,D, $p < 0.05$). The results of transwell assay mirrored that GNPAT1 overexpression obviously promoted but GNPAT1 knockdown significantly inhibited the migration and invasion of A549 and H1299 cells (Figure 3E-I, $p < 0.001$).

3.6 | GNPAT1 impacted cell migration-related protein expressions via upregulating vimentin, MMP-2, E2F1, and cyclin D1 expressions and downregulating E-cadherin and TIMP-2 expressions

We carried out Western blot to further observe the changes of the migration-related gene expressions (E-cadherin, vimentin, MMP-2, TIMP-2, E2F1, and cyclin D1) in A549 and H1299 cells under the impact of GNPAT1 overexpression or knockdown. As compared with the

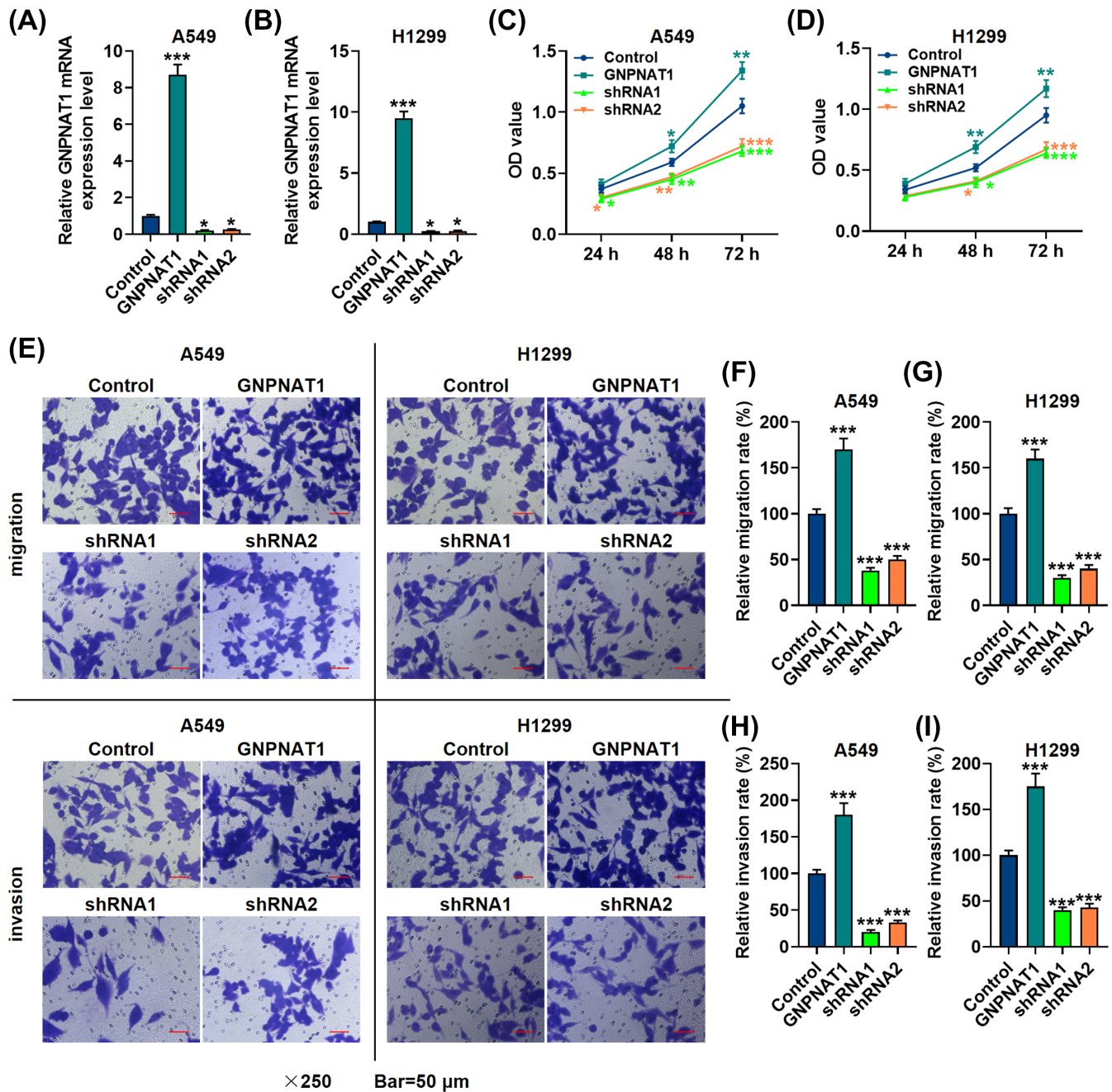


FIGURE 3 GNPAT1 promoted viability, migration and invasion of lung cancer cells. (A, B) Relative GNPAT1 mRNA expression was measured by RT-qPCR. GNPAT1 mRNA was overexpressed in GNPAT1 group, yet less expressed in shRNA1 and shRNA2 groups, as compared with that in the control group. (C, D) Cell viability was measured via CCK-8 assay at dedicated time intervals. Results of CCK-8 assay unraveled that OD value was greater in GNPAT1 group, but was smaller in shRNA1 and shRNA2 groups, when compared with that in control group within deterministic time intervals. (E-I) Relative migration and invasions rates. Transwell assays indicated that the migration and invasion of A549 and H1299 cells were explicitly augmented by GNPAT1 overexpression, while being markedly repressed by GNPAT1 knockdown. * $p < 0.05$, ** $p < 0.01$, *** $p < 0.001$ vs. Control. All results represent as means \pm standard deviation (SD) of triplicate determinations. RT-qPCR: real-time quantitative polymerase chain reaction, CCK-8: Cell Counting Kit-8.

control group, vimentin, MMP-2, E2F1, and cyclin D1 expressions were prominently increased in GNPAT1 group, while being apparently decreased in shRNA1 and shRNA2 groups (Figure 4A,B, $p < 0.01$). However, E-cadherin and TIMP-2 behaved in a diametrically opposite way, whose expression levels were reduced by overexpressed GNPAT1, but were fortified by GNPAT1 knockdown (Figure 4A,B, $p < 0.001$).

3.7 | GNPAT1 affected the xenograft tumor growth in vivo

The xenograft tumor mouse model was established. After the tumor was grown in mice for 28 days, the tumor was taken out (Figure 5A,D). As illustrated in Figure 5B,C,E,F, the tumor volume and tumor weight were

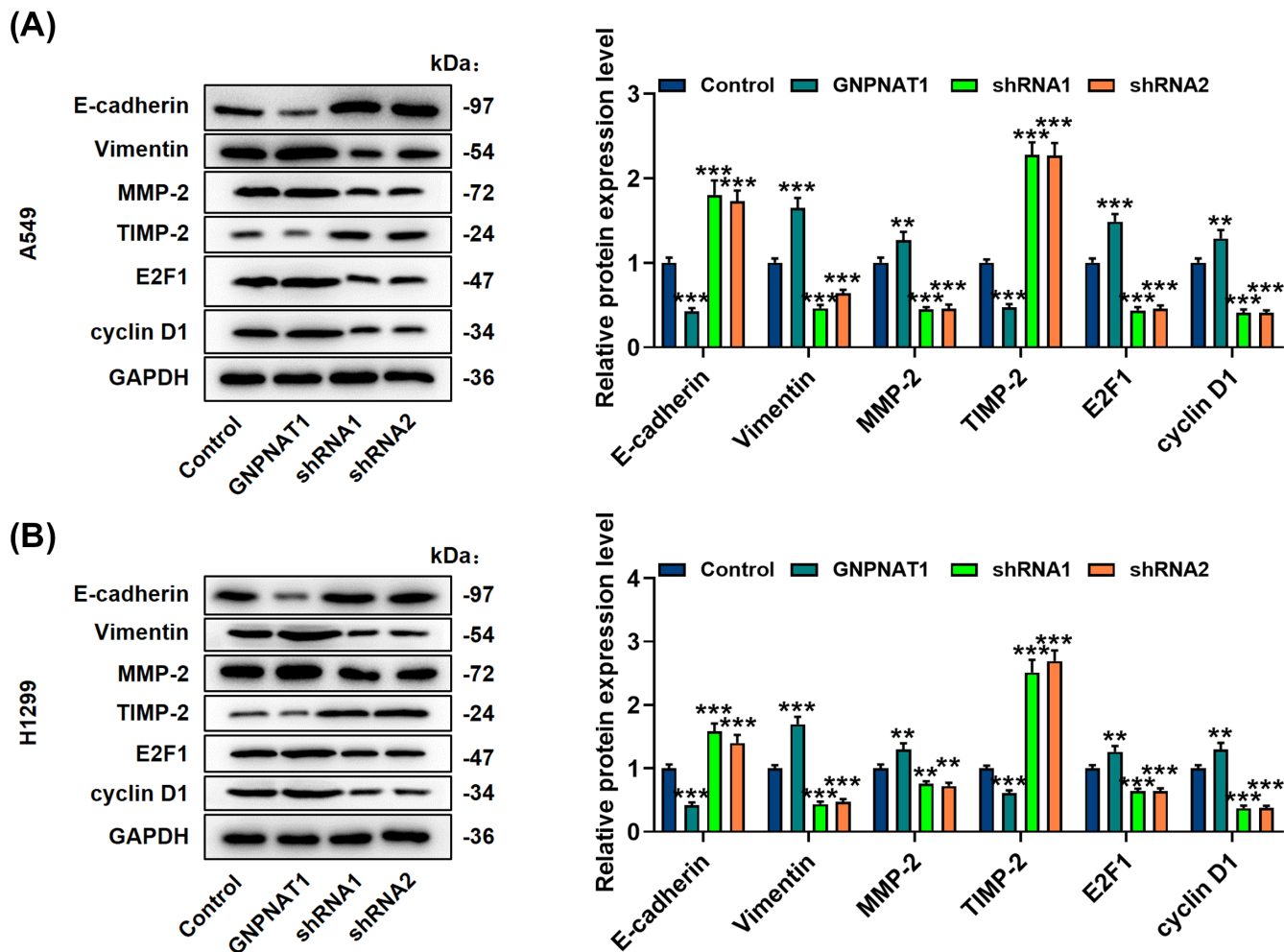


FIGURE 4 GNPAT1 impacted cell migration-related protein expressions via upregulating Vimentin, MMP-2, E2F1 and cyclin D1 expressions and downregulating E-cadherin and TIMP-2 expressions. (A, B) Expressions of cell migration-related proteins were measured via Western blot. Expressions of Vimentin, MMP-2, E2F1 and cyclin D1 were increased in GNPAT1 group, but were decreased in shRNA1 and shRNA2 groups. E-cadherin and TIMP-2 expression levels were reduced by GNPAT1 yet fortified by GNPAT1 knockdown. $**p < 0.01$, $***p < 0.001$ vs. Control. All results represent as means \pm standard deviation (SD) of triplicate determinations. MMP-2: Matrix metalloproteinase-2, TIMP-2: tissue inhibitor of metalloproteinase-2.

elevated in GNPAT1 group, whilst being lessened in shGNPNAT1 group, as compared to the control group ($p < 0.001$). Besides, the expression of GNPAT1 in tumor tissues was further examined using Western blot (Figure 5G-I) and immunohistochemistry (Figure 5J). It turned out that GNPAT1 overexpression upregulated the expression of GNPAT1 in tumor tissues, while shGNPNAT1 downregulated the expression of GNPAT1 in tumor tissues (Figure 5G-J, $p < 0.001$).

4 | DISCUSSION

Lung cancer, showing stubbornly high incidence and mortality, which ranks among the most deadly cancers worldwide.¹ Recently, much attention has been casted into the roles of gene markers on the basis of correlation with the prognosis predictions of lung cancer, as the rapid progress made in bioinformatics methodology.^{6,21,22} Additionally, interests in dysregulated metabolism of lung cancer

cells have emerged.^{23,24} Increasing studies put forward that aberrant GNPAT1 expression signifies carcinogenesis,²⁵ predicts poor prognosis,¹² and is related to proliferation of tumor cells.²⁶ However, the data are still limited, which require further enrichment or consolidation.

Researches against GNPAT1 have developed constantly and innovatively. Liu et al. presented that GNPAT1, together with other genes, exhibited inverse correlations with DNA methylation and expression,²⁷ which was expected to be one of the attractive and intriguing targets as the predictive biomarkers for cancers. Yang et al. conducted DNA methylation analyses on 8 elected genes to explore the feasibility in early diagnosis of lung cancer, GNPAT1 included.²⁸ Li et al. pointed out that the methylation detection on RASSF1A and SHOX2 genes was much more practicable than other methods in lung cancer diagnosis, particularly for the early stage diagnosis.²⁹ Nonetheless, no successor followed the independent study of GNPAT1 and DNA methylation in lung

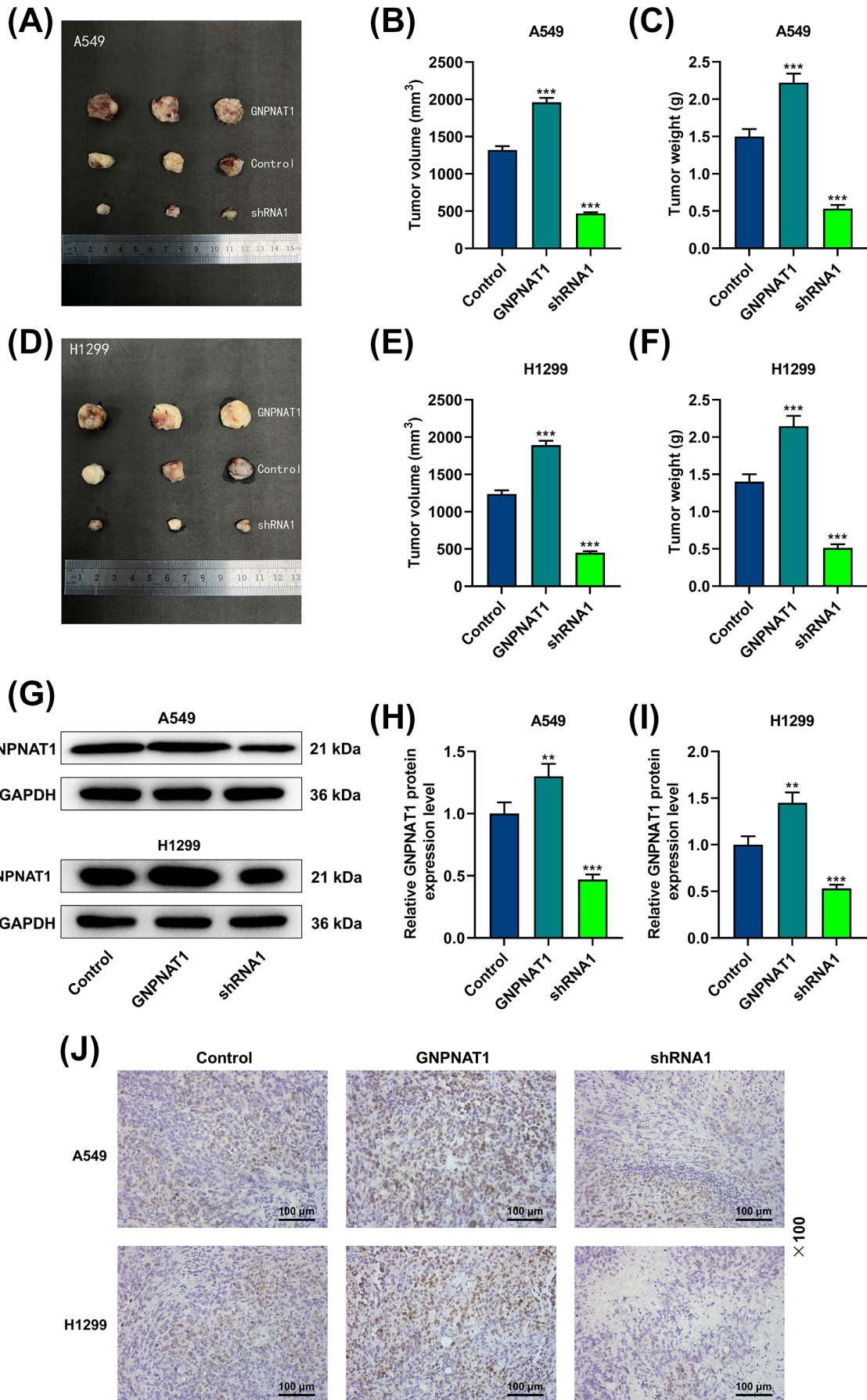


FIGURE 5 GNPAT1 affected the xenograft tumor growth in vivo. (A, F) After the xenograft tumor was grown in mice for 28 days, the tumor was taken out. The representative pictures of tumors were exhibited (A, D). The tumor volume (B, E) and tumor weight (C, F) were documented. (G-J) The expression of GNPAT1 in tumor tissue was detected by Western blot (G-I) and immunohistochemistry (J). ** $p < 0.01$, *** $p < 0.001$ vs. Control.

carcinoma and no research displayed the effects of GNPAT1 methylation on lung cancer irrespective of the reversibility of DNA methylation.³⁰ Li et al. highlighted the significance of P16 promoter methylation as one of the epigenetic changes, and stressed the clinical functions of P16 in lung cancer.³¹ In this sense, this would be the first time to uncover the correlations between GNPAT1 and DNA methylation in lung carcinoma and the functions of GNPAT1 on tumor cells, as supported by the consequence that significantly lower rate of GNPAT1 methylation existed in carcinoma tissues against para-carcinoma tissues, and the detected lower methylation coverage corresponded to the higher GNPAT1 expression. These findings suggested that GNPAT1 DNA hypomethylation or hypermethylation or the aberrant expressions are the potential indicators warning or reminding the progression and evolvement of lung cancer.

Echoed with the above studies, our research discovered according to the clinical data that the lower methylation of GNPAT1 in carcinoma tissues was associated with the worse prognosis of patients, and the methylation and expression levels of GNPAT1 significantly differed in carcinoma tissues and para-carcinoma tissues, implying that methylation level of GNPAT1 and its mRNA expressions may be underlying novel predictors for the prognosis of lung cancer patients. Besides, the methylation level was linked to tumor size, clinical stages, and lymph node metastasis. On the one hand, we found that GNPAT1 stimulated malignant cell viability, migration and invasion through CCK-8 assay as well as transwell assay. On the other hand, vimentin, MMP-2, E2F1 and cyclin D1 are participators in tumor development,³²⁻³⁵ and we discovered their expressions were prominently upregulated by GNPAT1, but apparently downregulated by GNPAT1 knockdown. However, E-cadherin and TIMP-2, enemies of tumor cells,^{36,37} appeared in an opposite way, whose expression levels were diminished by GNPAT1 yet enhanced by GNPAT1 knockdown. The changed expressions suggested GNPAT1 might act as a tumor promoter in lung cancer, supporting the conclusions as shown in clinical data. This finding coincided with the result of Zhang et al.²⁵ Furthermore, the enhancing effect of GNPAT1 on lung cancer discovered in vitro was further verified by the in vivo animal experiments, with the evidence that GNPAT1 overexpression promoted the growth of xenograft tumor, while GNPAT1 downregulation did the opposite.

To be emphasized, our study was conducted on A549 and H1299 cells, and validation experiments could be proceeded on other lung cancer cells. Besides, further studies were expected to exploit for fathoming out whether the downregulation of GNPAT1 expression or upmethylation agents could be applied for lung cancer treatment as therapeutic entity in terms of feasibility and practicability.

5 | CONCLUSIONS

Taken together, the above findings, together with the data present in this study, suggested the important roles of GNPAT1 expression in cancer germination and progression, and the expressions and the methylation level of GNPAT1 could serve as novel biomarkers for therapy and prognosis of lung cancer.

ACKNOWLEDGMENTS

Not applicable.

FUNDING INFORMATION

This work is supported by Shenzhen Key Medical Discipline Construction Fund (No.SZXX018).

CONFLICT OF INTEREST

The authors declare no conflicts of interest.

DATA AVAILABILITY STATEMENT

The data sets generated and/or analyzed during the current study are available from the corresponding author on reasonable request.

ORCID

Guofeng Li  <https://orcid.org/0000-0002-3806-0493>

REFERENCES

- Gao J, Qiu X, Xi G, et al. Downregulation of GSDMD attenuates tumor proliferation via the intrinsic mitochondrial apoptotic pathway and inhibition of EGFR/Akt signaling and predicts a good prognosis in nonsmall cell lung cancer. *Oncol Rep*. 2018;40(4):1971-1984.
- Zheng X, Li Y, Ma C, et al. Independent Prognostic Potential of GNPAT1 in Lung Adenocarcinoma. *Biomed Res Int*. 2020;2020:8851437-8851416.
- Siegel RL, Miller KD, Fuchs HE, Jemal A. Cancer Statistics, 2021. *CA Cancer J Clin*. 2021;71(1):7-33.
- Biomarkers Definitions Working G. Biomarkers and surrogate endpoints: preferred definitions and conceptual framework. *Clin Pharmacol Ther*. 2001;69(3):89-95.
- Jones GS, Baldwin DR. Recent advances in the management of lung cancer. *Clin Med (Lond)*. 2018;18(Suppl 2):s41-s46.
- Seijo LM, Peled N, Ajona D, et al. Biomarkers in Lung Cancer Screening: Achievements, Promises, and Challenges. *J Thorac Oncol*. 2019;14(3):343-357.
- Moore LD, Le T, Fan G. DNA methylation and its basic function. *Neuropsychopharmacology*. 2013;38(1):23-38.
- Mehta A, Dobersch S, Romero-Olmedo AJ, Barreto G. Epigenetics in lung cancer diagnosis and therapy. *Cancer Metastasis Rev*. 2015;34(2):229-241.
- Fraga MF, Ballestar E, Villar-Garea A, et al. Loss of acetylation at Lys16 and trimethylation at Lys20 of histone H4 is a common hallmark of human cancer. *Nat Genet*. 2005;37(4):391-400.

10. Clermont PL, Parolia A, Liu HH, Helgason CD. DNA methylation at enhancer regions: Novel avenues for epigenetic biomarker development. *Front Biosci (Landmark Ed)*. 2016;21:430-446.
11. Hao X, Luo H, Krawczyk M, et al. DNA methylation markers for diagnosis and prognosis of common cancers. *Proc Natl Acad Sci U S A*. 2017;114(28):7414-7419.
12. Liu W, Jiang K, Wang J, Mei T, Zhao M, Huang D. Upregulation of GNPAT1 Predicts Poor Prognosis and Correlates With Immune Infiltration in Lung Adenocarcinoma. *Front Mol Biosci*. 2021;8:605754.
13. Zhang J, Zhang J, Yuan C, et al. Establishment of the Prognostic Index Reflecting Tumor Immune Microenvironment of Lung Adenocarcinoma Based on Metabolism-Related Genes. *J Cancer*. 2020;11(24):7101-7115.
14. Yu X, Zhang X, Zhang Y. Identification of a 5-Genes Metabolic Signature for Predicting Prognosis Based on an Integrated Analysis of Tumor Microenvironment in Lung Adenocarcinoma. *J Oncol*. 2020;2020:5310793-5310712.
15. Liberti MV, Locasale JW. The Warburg Effect: How Does it Benefit Cancer Cells? *Trends Biochem Sci*. 2016;41(3):211-218.
16. Vander Heiden MG, Cantley LC, Thompson CB. Understanding the Warburg effect: the metabolic requirements of cell proliferation. *Science*. 2009;324(5930):1029-1033.
17. Huang da W, Sherman BT, Lempicki RA. Systematic and integrative analysis of large gene lists using DAVID bioinformatics resources. *Nat Protoc*. 2009;4(1):44-57.
18. Zhang C, Yu W, Wang L, et al. DNA Methylation Analysis of the SHOX2 and RASSF1A Panel in Bronchoalveolar Lavage Fluid for Lung Cancer Diagnosis. *J Cancer*. 2017;8(17):3585-3591.
19. Livak KJ, Schmittgen TD. Analysis of relative gene expression data using real-time quantitative PCR and the 2(-Delta Delta C[T]) Method. *Methods (San Diego, Calif)*. 2001;25(4):402-408.
20. Yoshioka M, Matsutani T, Hara A, et al. Real-time methylation-specific PCR for the evaluation of methylation status of MGMT gene in glioblastoma. *Oncotarget*. 2018;9(45):27728-27735.
21. Villalobos P, Wistuba II. Lung Cancer Biomarkers. *Hematol Oncol Clin North Am*. 2017;31(1):13-29.
22. Vargas AJ, Harris CC. Biomarker development in the precision medicine era: lung cancer as a case study. *Nat Rev Cancer*. 2016;16(8):525-537.
23. Papagiannakopoulos T, Bauer MR, Davidson SM, et al. Circadian Rhythm Disruption Promotes Lung Tumorigenesis. *Cell Metab*. 2016;24(2):324-331.
24. Sun Y, Huo C, Qiao Z, et al. Comparative Proteomic Analysis of Exosomes and Microvesicles in Human Saliva for Lung Cancer. *J Proteome Res*. 2018;17(3):1101-1107.
25. Zhang S, Zhang H, Li H, Guo J, Wang J, Zhang L. Potential role of glucosamine-phosphate N-acetyltransferase 1 in the development of lung adenocarcinoma. *Aging (Albany NY)*. 2021;13(5):7430-7453.
26. Kaushik AK, Shojaie A, Panzitt K, et al. Inhibition of the hexosamine biosynthetic pathway promotes castration-resistant prostate cancer. *Nat Commun*. 2016;7:11612.
27. Bacos K, Gillberg L, Volkov P, et al. Blood-based biomarkers of age-associated epigenetic changes in human islets associate with insulin secretion and diabetes. *Nat Commun*. 2016;7:11089.
28. Yang Z, Qi W, Sun L, Zhou H, Zhou B, Hu Y. DNA methylation analysis of selected genes for the detection of early-stage lung cancer using circulating cell-free DNA. *Adv Clin Exp Med*. 2019;28(3):355-360.
29. Li N, Zeng Y, Huang J. Signaling pathways and clinical application of RASSF1A and SHOX2 in lung cancer. *J Cancer Res Clin Oncol*. 2020;146(6):1379-1393.
30. Hyun J, Jung Y. DNA Methylation in Nonalcoholic Fatty Liver Disease. *Int J Mol Sci*. 2020;21(21):8138.
31. Li Y, Zhang T, Zhang H, et al. Clinical Significance of P16 Gene Methylation in Lung Cancer. *Adv Exp Med Biol*. 2020;1255:133-142.
32. Satelli A, Li S. Vimentin in cancer and its potential as a molecular target for cancer therapy. *Cell Mol Life Sci*. 2011;68(18):3033-3046.
33. Hadler-Olsen E, Winberg JO, Uhlén-Hansen L. Matrix metalloproteinases in cancer: their value as diagnostic and prognostic markers and therapeutic targets. *Tumour Biol*. 2013;34(4):2041-2051.
34. Sun CC, Zhou Q, Hu W, et al. Transcriptional E2F1/2/5/8 as potential targets and transcriptional E2F3/6/7 as new biomarkers for the prognosis of human lung carcinoma. *Aging (Albany NY)*. 2018;10(5):973-987.
35. Gautschi O, Ratschiller D, Gugger M, Betticher DC, Heighway J. Cyclin D1 in non-small cell lung cancer: a key driver of malignant transformation. *Lung Cancer*. 2007;55(1):1-14.
36. Toiyama Y, Yasuda H, Saigusa S, et al. Increased expression of Slug and Vimentin as novel predictive biomarkers for lymph node metastasis and poor prognosis in colorectal cancer. *Carcinogenesis*. 2013;34(11):2548-2557.
37. Bourbouli D, Han H, Jensen-Taubman S, et al. TIMP-2 modulates cancer cell transcriptional profile and enhances E-cadherin/beta-catenin complex expression in A549 lung cancer cells. *Oncotarget*. 2013;4(1):166-176.

How to cite this article: Ding P, Peng B, Li G, Sun X, Wang G. Glucosamine-phosphate N-acetyltransferase 1 and its DNA methylation can be biomarkers for the diagnosis and prognosis of lung cancer. *J Clin Lab Anal*. 2022;36:e24628. doi: [10.1002/jcla.24628](https://doi.org/10.1002/jcla.24628)